



HAL
open science

Radiation damage in ceria

Jean-Marc Costantini

► **To cite this version:**

Jean-Marc Costantini. Radiation damage in ceria. Exploratory Materials Science Research, 2020, 1, pp.1-6. 10.47204/EMSR.1.1.2020.001-006 . cea-03186648

HAL Id: cea-03186648

<https://cea.hal.science/cea-03186648>

Submitted on 31 Mar 2021

HAL is a multi-disciplinary open access archive for the deposit and dissemination of scientific research documents, whether they are published or not. The documents may come from teaching and research institutions in France or abroad, or from public or private research centers.

L'archive ouverte pluridisciplinaire **HAL**, est destinée au dépôt et à la diffusion de documents scientifiques de niveau recherche, publiés ou non, émanant des établissements d'enseignement et de recherche français ou étrangers, des laboratoires publics ou privés.

Radiation Damage in Ceria

Jean-Marc COSTANTINI

Université Paris-Saclay, CEA, Service de Recherches Métallurgiques Appliquées, 91191, Gif-sur-Yvette, France

ABSTRACT

The damage induced in cerium dioxide or ceria by charged particle irradiations was investigated by various spectroscopic techniques, such as Raman spectroscopy, electron paramagnetic resonance (EPR) spectroscopy, and UV-visible absorption/reflection spectroscopy. These results confirmed the radiation resistance of this material which is not amorphised by heavy ion irradiations even for high fluence and high stopping power. However, clear evidence of cerium reduction from the 4+ to 3+ oxidation state was provided by EPR and optical spectroscopy data after electron or heavy ion irradiations.

I. INTRODUCTION

Cerium dioxide (CeO_2) or ceria is an important material for applications to solid oxide fuel cells (SOFC) and catalysis, for which the oxygen non-stoichiometry plays a great role [1]. It can be envisioned as a non-radioactive surrogate of the actinide dioxides with the cubic fluorite-type structure, such as plutonia (PuO_2) with the 4+ oxidation state of Pu [2]. Moreover, Ce and the transuranium elements (Pu, Am and Cm) share the same 3+ and 4+ oxidation states in oxides. The sesquioxides (M_2O_3) are indeed found for trivalent actinides [2] as well as for rare earths [3]. Furthermore, the 5f electrons become more localized starting with Pu in the actinide series [4], just like the 4f electrons in the lanthanide series in the normal conditions. Therefore, the knowledge of radiation damage in ceria is an important topic for applications to nuclear fuel and nuclear waste behaviour.

Ceria is known as a radiation-resistant material, just like urania (UO_2) and yttria-stabilized zirconia (ZrO_2 : Y) with the same fluorite-type structure that cannot be amorphised either by displacement damage or by ionization [5]. Many studies were dedicated to the radiation damage in ceria by using various experimental techniques, such as X-ray Diffraction (XRD) [6, 7], X-ray absorption spectroscopy [7], transmission electron microscopy (TEM) [8], and scanning transmission electron microscopy (STEM) [9]. In this respect, the study of disorder at different length scales is an important issue for such non-amorphisable materials. Therefore, we have tried to tackle this issue by using spectroscopies giving information on different length scales in electron and ion irradiated ceria.

Raman spectroscopy data definitely show that ceria is not amorphised by swift heavy ion irradiations. Electron paramagnetic resonance (EPR) and UV-visible optical absorption/reflection spectroscopy confirm this conclusion and show clear evidence of the reduction of Ce^{4+} to Ce^{3+} induced by electron or ion irradiations, either due to nuclear-collision or electronic-excitation processes. The respective roles of point-defect formation and electron-hole pair production are addressed in this brief review of our recent results.

II. EXPERIMENTAL DETAILS

Tiny single crystals (about 1 mm in thickness) and sintered samples of ceria with 150- μm thickness were used for this study. The single crystals show triangular facets corresponding to the {111} growth planes. Irradiations of the single crystals were carried out near room temperature (RT) with electrons of energies from 1.0 MeV to 2.5 MeV for several

fluences. Irradiations of sintered samples were also performed near RT with high-energy heavy ion beams (Kr, Xe, W, Au) for various energies and fluences. The irradiation parameters such as stopping power and range for the different incident particles computed with the SRIM2013 code [10] are displayed in Table I.

Table I: Nuclear (S_n) and electronic (S_e) stopping power and range for the different incident particles, computed with the SRIM2013 code [9].

Particle	Energy (MeV)	Range (μm)	S_n (keV nm ⁻¹)	S_e (keV nm ⁻¹)
e ⁻	1.0	9x10 ³		9x10 ⁻⁴
e ⁻	1.4	1.4x10 ⁴		9.2x10 ⁻⁴
e ⁻	2.5	2.5 x10 ⁴		1x10 ⁻³
⁸² Kr	100	9.1	0.064	17
¹³¹ Xe	200	11.8	0.011	27.5
¹⁸³ W	10	1.3	5	2.1
¹⁸³ W	36	3.8	12	0.1

In view to study the damage at different length scales in these irradiated samples, we have used various experimental techniques such as on-line and off-line micro-Raman spectroscopy at RT, UV-visible optical absorption and reflection spectroscopy at RT, and X-band EPR spectroscopy down to low temperature (4.3 K). All experimental details on sample preparation and measurements can be found in the cited references [11-14].

III. RESULTS AND DISCUSSION

III.1. Raman spectroscopy

These data provide information about the disorder at the level of bonds. Since Raman scattering is dependent on the polarizability tensor, it probes the centrosymmetric optical phonon modes of the lattice. Selection rules impose that only the modes at the centre of Brillouin zone can be Raman-active in a periodic solid. However, two-phonon or overtones and combination modes can also be allowed. Lattice disorder and defects can also render Raman-active some modes that would be otherwise forbidden [15].

Measurements by micro-Raman spectroscopy with 532-nm Nd-YAG laser excitation were performed on single grains (~10 μm) of the sintered samples irradiated with heavy ions. The Raman spectra show the decrease versus fluence of the Raman-allowed centre-of-zone T_{2g} phonon peak at 467 cm⁻¹ (Figure 1) [11] which is the characteristic feature of the fluorite structure, just like for urania [16]. The five satellite peaks near the main T_{2g} peak were assigned to the oxygen deficiency. The second-order peaks (not shown) and the satellites also decayed as a function of fluence (Figure 1).

The damage fraction (f_D) was deduced from the relative decrease of the T_{2g} peak intensity (Figure 2). It is seen that f_D shows saturation at ~45%, thereby proving the radiation resistance of ceria which is not amorphised by such swift heavy ion irradiations for electronic stopping powers up to ~28 keV nm⁻¹ (Table I).

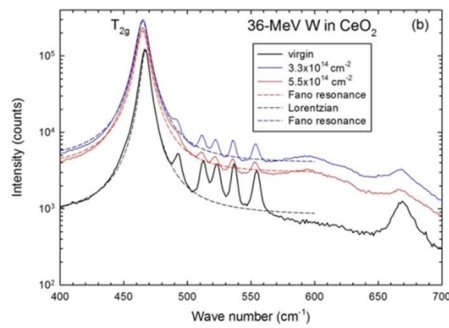


Figure 1: Off-line Raman spectra of virgin and 36-MeV W ion-irradiated ceria samples for various ion fluences. The Lorentzian and Fano line shapes were used to fit the T_{2g} peaks of the virgin and irradiated samples, respectively (dashed lines). The spectrum of the virgin sample was down-shifted for sake of clarity [11].

The asymmetry of the T_{2g} peak appearing after irradiation (Figure 1) was assigned to different origins, such as a Fano resonance effect and the formation of oxygen vacancies. Yet, no clear cut conclusions could be drawn from these data. However, an extra broad band was recorded at $\sim 600 \text{ cm}^{-1}$ that could also be associated to oxygen vacancies (Figure 1) [17]. Damage cross sections were then deduced from the decrease of f_0 versus fluence for the various electronic stopping power values (Figure 2) by using a saturation function. The inelastic thermal spike model was applied to reproduce the dependence of the track cross section on the electronic stopping power (Figure 3). The contribution of nuclear collisions was also included for the lower energy ions (10-MeV W). The present data are quite consistent with previous results based on XRD [6] and conventional TEM [8] (Figure 3). However, large deviations are found with STEM results [9] giving much smaller values of the track core radii.

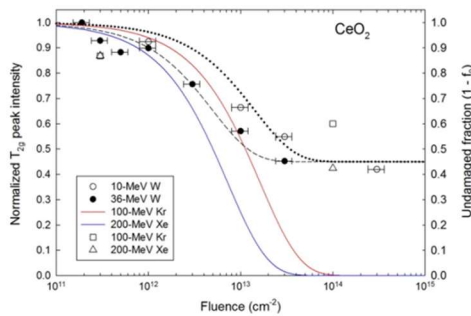


Figure 2: Normalized T_{2g} peak intensity for the W ion irradiations (left scale), and undamaged fraction ($1 - f_0$) for Kr and Xe ion irradiations deduced from STEM [8] (solid lines, right scale) as a function of fluence. Dashed and dotted lines are fits of W-ion data with a saturation function for 36-MeV and 10-MeV energies, respectively [11].

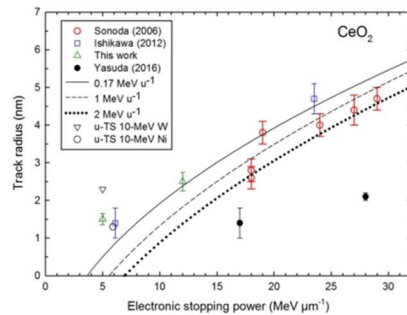


Figure 3: Experimental radii versus electronic energy loss from Sonoda et al. [8], Ishikawa et al. [6], Yasuda et al. [9], and the present data [11]. The lines are inelastic thermal spike calculations for the three different beam energies of 0.17, 1.0 and 2.0 MeV u^{-1} . Open triangles and open circles are calculations (u-TS) combining the electronic and nuclear energy losses for 10-MeV W and 10-MeV Ni ions [11].

III.2. EPR and optical spectroscopy

These data give insight on modifications at the atomic level and evolution of the electronic structure. Measurements by X-band EPR spectroscopy and UV-visible absorption spectroscopy were carried out on electron-irradiated single crystals and UV-visible optical reflection spectroscopy on heavy ion irradiated sintered samples. Evidence of Ce^{3+} ion formation was provided by EPR spectroscopy at 4.3 K with the applied magnetic field lying in a {111} facet of the single crystals irradiated with 2.5-MeV electrons for a fluence of $1.5 \times 10^{18} \text{ cm}^{-2}$ (Figure 4) [12]. Spectra were showing narrow lines for g-factor values of ~ 1.3 for electron energies larger than or equal to 1.4 MeV. No such signal was found for 1.0-MeV electron irradiation for the same high fluence and similar inelastic stopping power (Table I). By rotating the crystal in the {111} plane with respect to the applied magnetic field, the lines followed a typical sinewave angular variation with a weak g-factor anisotropy ($\Delta g \sim 0.3$).

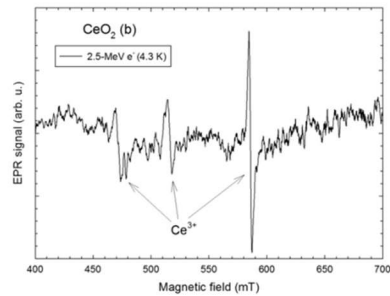


Figure 4: X-band EPR spectra after baseline correction at 4.3 K of a CeO_2 single crystal irradiated with 2.5-MeV electrons at a fluence of $1.5 \times 10^{18} \text{ cm}^{-2}$ with the applied magnetic field parallel to a {111} plane [12].

These lines vanished when temperature was raised above 10 K, which is the signature of a short spin-lattice relaxation time leading to broadening due to fast relaxation when more phonons are emitted and absorbed at higher temperature. All these results are consistent with the $4f^1$ state of cerium, corresponding to Ce^{3+} . The occurrence of narrow lines at low temperature with a definite trigonal anisotropy shows that the crystalline order is kept at the atomic scale in the next-neighbour shell around Ce^{3+} ions, which is consistent with the conclusions of Raman spectroscopy.

This reduction process was related to cerium displacement not to oxygen displacement, since it occurs only for electron energies larger than or equal to 1.4 MeV [12, 13] by using the admitted displacement threshold energy $E_d(\text{Ce})$ of 58 eV [18]. The displacement cross sections for oxygen atoms is of $\sigma_d(\text{O}) \sim 13 \text{ b}$ for the 1.0-MeV energy, and $\sigma_d(\text{O}) \sim 16 \text{ b}$ for the 1.4-MeV energy by using a recommended value of $E_d(\text{O}) = 35 \text{ eV}$ [18]. As a result, the formation of Ce^{3+} ions cannot be attributed to oxygen displacement. No signals of paramagnetic oxygen vacancies with the 1+ charge state ($\text{V}_\text{O}^\bullet$ or F^+ centres) or oxygen hole centres near $g \sim 2$ were recorded whatsoever.

Optical reflection spectroscopy data on ion-irradiated sinters recorded at RT showed the appearance of six bands after subtraction of the virgin sample spectrum (Figure 5) [14]. Three of those bands, centred at ~ 1.2 , 2.2 and 2.8 eV (i. e. ~ 9500 , 18000, 23000 cm^{-1}), were recorded for the reference spectrum with an optical gap of $\sim 3.2 \text{ eV}$ ($\sim 26000 \text{ cm}^{-1}$) generally assigned to $2p \rightarrow 4f$ transitions. The latter three bands and the three other bands centred at ~ 4.0 , 4.8, and 6.2 eV (i. e. ~ 33000 , 39000, 50000 cm^{-1}) were found to grow after ion irradiation. Analysis of the possible electronic transitions allowed assigning the first three bands to $4f \rightarrow 5d$ transitions for low photon energies and the other three ones to $2p \rightarrow 5d$ transitions for high photon energies [14].

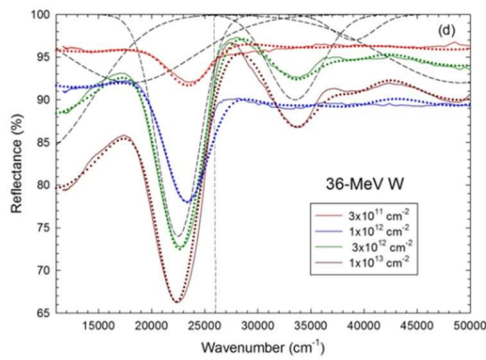


Figure 5: UV-visible differential reflection spectra of ceria sintered samples after irradiation for various fluences with 36-MeV W. The dotted curves are trial-and-error fits with six Gaussian profiles. The dashed curves are the fitted bands. The vertical dashed line marks the optical gap value ($\sim 26,000 \text{ cm}^{-1}$) [14].

Those bands are growing due to an increase of the amount of Ce^{3+} associated to oxygen vacancies that break and lower the spherical local symmetry around Ce^{3+} ions. The enhancement of oxygen vacancies (V_{O}) with respect to the pristine samples was assumed to arise from nuclear collisions. The axial symmetry caused by neighbouring V_{O} induces a splitting of the empty 5d levels of Ce^{4+} into three levels by the crystal field interactions. The three $2p \rightarrow 5d$ extra transitions that were not found in the virgin sample are related to the significant increase of Ce^{3+} ions and oxygen vacancies due to ion irradiation. These reflection spectra were converted to absorption spectra for the W ions at the fluence of saturation (Figure 6).

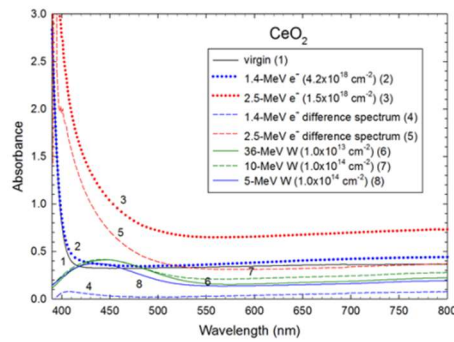


Figure 6: UV-visible absorption spectra of electron-irradiated ceria single crystals (1 to 5) [12-13] with the absorbance deduced from reflection spectra of W-ion irradiated ceria sinters for the maximum fluences at saturation (6 to 8) [14].

The reflection spectra are all showing a bump at $\sim 440 \text{ nm}$ (i. e. $\sim 23000 \text{ cm}^{-1}$) which is consistent with the absorption spectra of electron-irradiated single crystals showing a broad absorption tail below the absorption edge at $\sim 3.2 \text{ eV}$ ($\sim 400 \text{ nm}$) for 1.4-MeV and 2.5-MeV energies and not for the 1.0-MeV energy [13] (Fig. 6). This is in agreement with the conclusions of EPR data [12], provided that oxygen vacancies are EPR-silent, i. e. non paramagnetic species, either neutral (V_{O}^{\times}), with two electrons, or with the 2+ charge state ($V_{\text{O}}^{\cdot\cdot}$), devoid of electrons. Some *ab-initio* calculations have actually shown that clusters such as the $(\text{Ce} - V_{\text{O}}^{\cdot\cdot})$ dimers and $(\text{Ce} - V_{\text{O}}^{\cdot\cdot} - \text{Ce})$ trimers are the dominant defect species for low oxygen potential [19].

From the dependence of the band intensities on ion fluence, damage cross sections were deduced as a function of the electronic stopping power (Figure 7). Those cross sections are much larger than the values deduced from Raman spectra (Figure 2). No correlation was found with the nuclear stopping power whatsoever. The growth of bands is found up to saturation for high stopping power values (Figure 7).

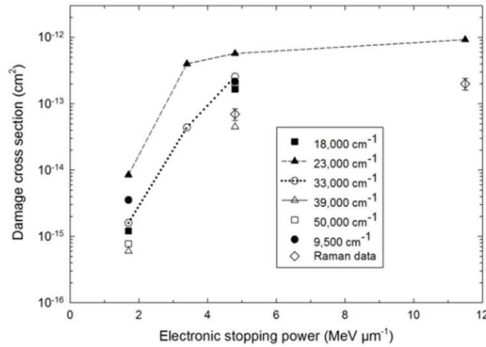


Figure 7: Damage cross sections deduced from the growth curves of the various bands in reflection spectra and from the T_{2g} peak intensity in Raman spectra (open diamonds) [11] versus electronic stopping power (S_e) (Table I). Lines are guides to the eyes.

A kinetic model was devised to interpret these data on the basis of the electron-hole pair generation by above the 2p–5d band-gap electronic excitations ($E_g \sim 6$ eV) [14]. The rate equations represent the competition between free hole trapping on Ce^{3+} and free electron trapping on Ce^{4+} . The dependence of the Ce^{3+} content on fluence deduced from these equations exhibit saturation behaviour. The saturation of cross sections versus stopping power corresponds to the equilibrium state between these two electronic processes.

As such, the “damage cross sections” deduced from reflection spectra must be considered as effective values including the latter electronic processes, and not reflecting any damage measured by Raman spectroscopy, or other techniques such as TEM. Our results show the complex nature of radiation damage in a material like ceria, since it is not undergoing striking structural modifications, such as amorphisation or phase change. The relevance of spectroscopies is highlighted in the present work, since these techniques can provide direct information of the material’s evolution at a microscopic level and allow the benchmark of simulations of defect formation.

IV. CONCLUSIONS

All these experimental results obtained for the different length scales of the material confirm the radiation resistance of ceria. In particular, no evidence of amorphisation after electron or heavy ion irradiations was found whatsoever. However, the Ce reduction from the 4+ to the 3+ oxidation state is induced either by elastic collisions in electron-irradiated single crystals (due to Ce atom displacement), or by electronic excitations (due to free electron trapping on Ce^{4+} lattice ions) in ion-irradiated sintered samples.

REFERENCES

- [1] M. Belmonte, *Adv. Engineer. Mater.* **8**, 693 (2006).
- [2] L. Petit, A. Svane, Z. Szotek, W. M. Temmerman, and G. M. Stocks, *Phys. Rev. B* **81**, 045108 (2010).
- [3] G. Adachi, and N. Imanaka, *Chem. Rev.* **98**, 1479 (1998).
- [4] T. Vitova , I. Pidchenko , D. Fellhauer , P. S. Bagus, Y. Joly, T. Pruessmann, S. Bahl, E. Gonzalez-Robles , J. Rothe , M. Altmaier , M. A. Denecke, and H. Geckeis, *Nature Commun.* **8**, 16053 (2017).
- [5] J.-M. Costantini, F. Beuneu, and W. J. Weber, "*Radiation Damage in Cubic-Stabilized Zirconia and Ceria*", in "*Properties of Fluorite Structure Materials*", Eds. P. Vajda and J. M. Costantini (Nova Science Publishers, New York, 2013), pp. 127-152.
- [6] N. Ishikawa, and K. Takegahara, *Nucl. Instr. and Meth. B* **272**, 227 (2012).
- [7] C. L. Tracy, M. Lang, J. M. Pray, F. Zhang, D. Popov, C. Park, C. Trautmann, M. Bender, D. Severin, V. A. Skuratov, R.C. Ewing, *Nat. Commun.* **6**, 6133 (2015).
- [8] T. Sonoda, M. Kinoshita, N. Ishikawa, M. Sataka, Y. Chimi, and A. Iwase, *Nucl. Instr. and Meth. B* **250**, 254 (2006).
- [9] S. Takaki, K. Yasuda, T. Yamamoto, S. Matsumura, and N. Ishikawa, *Progress in Nucl. Energy* **92**, 306 (2016).
- [10] J. P. Biersack, and L. G. Haggmark, *Nucl. Instr. and Meth.* **174**, 257 (1980) (www.srim.org).
- [11] J.-M. Costantini, S. Miro, G. Gutierrez, K. Yasuda, S. Takaki, N. Ishikawa, and M. Toulemonde, *J. Appl. Phys.* **122**, 205901 (2017).
- [12] J.-M. Costantini, L. Binet, N. Touati, G. Lelong, M. Guillaumet, and W. J. Weber, *J. Appl. Phys.* **123**, 025901 (2018).
- [13] J.-M. Costantini, G. Lelong, M. Guillaumet, W. J. Weber, S. Takaki, and K. Yasuda, *J. Phys.: Condens. Matter* **28**, 325901 (2016).
- [14] J.-M. Costantini, G. Lelong, M. Guillaumet, D. Gourier, S. Takaki, N. Ishikawa, H. Watanabe, and K. Yasuda, *J. Appl. Phys.* **126**, 175902 (2019).
- [15] M. H. Brodsky, and M. Cardona, *J. Non-Crystal. Solids* **31**, 81 (1978).
- [16] P. R. Graves, *Appl. Spectrosc.* **44**, 1665 (1990).
- [17] K. Ohhara, N. Ishikawa, S. Sakai, Y. Matsumoto, O. Michikami, and Y. Ohta, *Nucl. Instr. and Meth. B* **267**, 973 (2009).
- [18] K. Yasunaga, K. Yasuda, S. Matsumura, and T. Sonoda, *Nucl. Instr. and Meth. B* **266**, 2877 (2008).
- [19] T. Zacherle, A. Schrieffer, R. A. de Souza, and M. Martin, *Phys. Rev. B* **93**, 134104 (2013).